3405

NACA RM L55I12

NACA

RESEARCH MEMORANDUM

LIFT, DRAG, AND LONGITUDINAL STABILITY AT MACH NUMBERS FROM 1.4 TO 2.3 OF A ROCKET-POWERED MODEL HAVING A 52.5° SWEPTBACK WING OF ASPECT RATIO 3 AND INLINE TAIL SURFACES

By Warren Gillespie, Jr.

Langley Aeronautical Laboratory
Langley Field, Va.

NATIONAL ADVISORY COMMITTEE FOR AERONAUTICS

WASHINGTON

December 15, 1955
Declassified January 27, 1960

NACA RM L55I12

NATIONAL ADVISORY COMMITTEE FOR AERONAUTICS

RESEARCH MEMORANDUM

LIFT, DRAG, AND LONGITUDINAL STABILITY AT MACH NUMBERS FROM 1.4 TO 2.3 OF A ROCKET-POWERED MODEL HAVING A 52.5° SWEPTBACK WING OF ASPECT RATIO 3 AND INLINE TAIL SURFACES

By Warren Gillespie, Jr.

SUMMARY

An investigation was made of a configuration having a body of fineness ratio 16.9, a 52.5° sweptback wing of aspect ratio 3, taper ratio 0.2, and NACA 65A004 airfoil section, and an inline tail which was aeropulsed continuously in pitch during free flight with and without a sustainer rocket motor operating. The Mach number range covered by the investigation was from 1.4 to 2.3. Zero-lift drag and drag-due-to-lift data were obtained during coasting flight of the model. Normal force, pitching moment, static longitudinal stability, and wash and wake effects at the horizontal tail were obtained with and without the rocket motor thrusting.

Model drag at zero lift was nearly the same as for a similar model with a 3-percent-thick unswept wing of hexagonal section and aspect ratio 3 (reported in NACA RM L55B10), but drag due to lift was approximately 11 to 25 percent higher. The variation of lift with angle of attack was linear over the angle-of-attack test range of ±5.5°. The variation of pitching moment with lift was also linear. Static stability decreased gradually with increasing Mach number. Upwash occurred at the horizontal tail at Mach numbers above 1.5 and angles of attack near ±1°. The maximum loss of effective dynamic pressure at the horizontal tail due to the wing wake was approximately 14 percent of the free-stream dynamic pressure. The continuous pitching of the model induced lateral oscillations having a maximum amplitude of about $\pm 2\frac{1}{2}^{\circ}$ of sideslip at a Mach number of 2.

INTRODUCTION

Supersonic tests of thin wings swept within the Mach cone have indicated that above a Mach number of about 1.6 only a small amount of the theoretical leading-edge suction force was developed at lifting conditions. (See refs. 1 to 5.) Leading-edge separation and compressibility are factors tending to reduce the magnitude of the suction force. At lower supersonic speeds the magnitude of the theoretical suction force is greater. A test of an aspect-ratio-3 delta wing on a body at Mach numbers up to 1.38 has shown that the maximum lift-drag ratios for the flat wing were approximately halfway between the ratios calculated for conditions of no leading-edge suction and full leading-edge suction (ref. 6). Recently, a 20-percent increase in maximum lift-drag ratio has been realized at a Mach number of 1.2 by the use of a particular method of applying twist and camber (ref. 7).

The results presented in this paper are part of a supersonic research program utilizing rocket-propelled models to investigate primarily the effect of wing configuration on drag due to lift, lift, and longitudinal stability characteristics. A previous model tested had a 3-percent-thick unswept wing of aspect ratio 3 and hexagonal airfoil section (ref. 8). The wing-off and body-alone characteristics have been reported in references 9 and 10, respectively.

In the present investigation a model having an aspect-ratio-3 wing with 52.5° quarter-chord sweep, taper ratio 0.2, and NACA 65A004 airfoil section, and an inline tail was flight tested at Mach numbers from 1.4 to 2.3 at the Langley Pilotless Aircraft Research Station at Wallops Island, Va. The horizontal tail was aerodynamically pulsed between stop settings of 2.03° and -1.83°. The basic aerodynamic parameters in pitch were determined from the continuous response of the model to the flip-flop tail motion.

SYMBOLS

C_N normal-force coefficient, $\frac{a_n}{g}\frac{W/S}{q}$

C_C chord-force coefficient, $\frac{-a_l}{g}\frac{W/S}{q}$

C_L lift coefficient, $C_N \cos \alpha - C_C \sin \alpha$

C_D drag coefficient, $C_C \cos \alpha + C_N \sin \alpha$

C_m	pitching-moment coefficient about $0.55\bar{c}$, $\frac{I_Y\ddot{\theta}}{57.3\ qS\bar{c}}$
a_n	normal acceleration, ft/sec^2
a_l	longitudinal acceleration, ft/sec^2
g	acceleration due to gravity, 32.2 ft/sec^2
q	dynamic pressure, lb/sq ft
V	velocity, ft/sec
M	Mach number
R	Reynolds number, where reference length is 1 ft
W	weight of model, lb
$\ddot{\theta}$	angular acceleration in pitch determined by two accelerometers, radians/sec^2
θ/L	streamwise wing twist due to 100-lb load at 0.50 chord, deg/100 lb (see fig. 9)
S	total wing area to body center line, 4.00 sq ft
b	wing span, ft
$\bar{c}$	wing mean aerodynamic chord, 1.32 ft
α	angle of attack, deg
β	angle of sideslip, deg
δ	horizontal-tail deflection, deg
I_Y	moment of inertia in pitch about center of gravity, slug-ft^2
q_t/q	ratio of effective dynamic pressure at horizontal tail to free-stream dynamic pressure

Subscripts:

e elastic wing

r rigid wing

MODEL

A drawing of the test configuration is shown in figure 1. The fuselage was a body of revolution of fineness ratio 16.9. Ordinates defining the nose shape are given in table I. The geometric and mass characteristics of the model are listed in table II. The ratio of the maximum diameter of the body to the wing span was 0.168. A 52.5° sweptback wing (25-percent-chord line) of aspect ratio 3 and taper ratio 0.2 and having an NACA 65A004 streamwise airfoil section was mounted on the body center line in line with the horizontal tail which was mass balanced and pivoted about the 0.55-exposed-mean-aerodynamic-chord point.

The model was of metal construction with a solid steel wing. A sustainer rocket motor was carried inside the fuselage in addition to a telemeter with angle-of-attack, angle-of-sideslip, pressure, and accelerometer instruments. The model and its booster are pictured in the launching attitude in figure 2.

TESTS

Data were obtained during ascent of the model after separation from the booster. During flight of the model alone, a square-wave pulse was continuously generated as the tail automatically flipped between stop settings because of a reversal in direction of the tail lift.

The quantities measured by the telemeter system were normal and longitudinal accelerations, angles of attack and sideslip, horizontal tail deflection, and total pressure. The velocity obtained from CW Doppler radar was used in conjunction with tracking radar and radiosonde data to calculate Mach number, Reynolds number, and dynamic pressure. Ground rollsonde equipment operating in conjunction with the directional telemeter antenna signal from the model indicated that the level of model rolling velocity was approximately 1 radian per second throughout the flight. The variation of the free-stream Reynolds number per foot length and dynamic pressure with Mach number is shown in figure 3(a). There was a coasting period before and after the period of flight with sustainer power on. The ranges of the maximum angles of attack and induced sideslip are shown in figure 3(b).

A solid aluminum-alloy wing panel having the same plan form and airfoil section as the steel wing of the flight model was static tested to measure the streamwise wing twist due to loading concentrated along the 50-percent-chord line. From this test a set of structural influence coefficients was determined for the wing of the flight model for use in estimating the aeroelastic reduction in wing lift encountered by the model during its flight.

ACCURACY AND CORRECTIONS

The random error in the data is indicated by the scatter of the experimental points. The probable error of a telemetered quantity obtained from a single instrument is approximately 1 percent of the calibrated instrument range. Presented below are the ranges of the telemeter instruments used in the test model:

Nose angle-of-attack indicator, deg	±10
Nose angle-of-sideslip indicator, deg	±5
Vertical-tail angle-of-sideslip indicator, deg	±6
Normal accelerometer at the nose, g units	±30
Normal accelerometer near the center of gravity, g units	±40
Longitudinal accelerometer, g units	±1 to -8
Total-pressure indicators at nose and tail, lb/sq in.	14 to 100
Horizontal-tail-position indicator, deg	±2.25

Further errors in aerodynamic coefficients may arise because of possible dynamic-pressure inaccuracies which are approximately twice as great as the errors in Mach number. The Mach numbers are estimated to be accurate to ±1 percent.

Examination of plots of the longitudinal-acceleration data against normal-acceleration data indicated an effective angular misalinement of about 1° for the longitudinal accelerometer. The effect of this misalinement on the determination of drag due to lift is discussed later in the section on drag.

An additional source of inaccuracy in the final results may be cross-coupling effects of induced sideslip and rolling motions. These effects as indicated by figure 3(b) would be expected to be somewhat greater at the higher supersonic test Mach numbers.

Measurements obtained from the wind-vane instruments were corrected for position error resulting from flight-path curvature. Position corrections were also made to measurements obtained from the normal and longitudinal accelerometers mounted near the center of gravity of the model. The loss in total pressure measured at the horizontal tail was converted

to an effective loss in dynamic pressure by assuming the local static pressure at the tail equal to free-stream static pressure and using the relation

$$\text{Effective loss in dynamic pressure, } \Delta q = \frac{\text{Loss in total pressure}}{1 + \frac{M^2}{4} + \frac{M^4}{40} + \frac{M^6}{1600}}$$

Then

$$\frac{q_t}{q} = 1 - \frac{\Delta q}{q}$$

RESULTS AND DISCUSSION

Drag

Figure 4 shows a drag polar at a Mach number of 1.50. The flagged symbols represent points corrected for angular misalinement of the longitudinal accelerometer mentioned previously. The variation shown by the solid line was obtained in the manner described in reference 8, by plotting the drag coefficient against C_L^2 and determining an average curve. The solid line and the flagged symbols gave very nearly the same drag polar for the basically symmetrical test model. Rather than correct each point individually for this misalinement effect, plots of drag coefficient against C_L^2 were made at different Mach numbers over the Mach number range of the test. Drag due to lift $\frac{dC_D}{dC_L^2}$ was determined from the slope of the average curve, and minimum drag was taken to occur at zero lift.

The variation with Mach number of the drag at zero lift is shown in figure 5(a). The drag at zero lift was nearly the same as for the model of reference 8 which had the same fuselage and tail and a 3-percent-thick unswept wing of hexagonal section, aspect ratio 3, and taper ratio 0.4.

Shown in figure 5(b) is the variation of drag due to lift. The expression $\frac{1}{57.3C_{N_\alpha}}$ gave higher drag up to a Mach number of about 2.3.

At a Mach number of 1.45 the difference is equal to approximately one-half of the theoretical leading-edge suction force (calculated from ref. 1). The drag due to lift for the present test model was approximately 11 percent higher than that of the unswept wing model of reference 8 at a Mach number of 1.5 and 25 percent higher at a Mach number of 2.0. Insofar as drag due to lift is concerned, the swept wing model appears to be relatively inefficient.

In this connection it is interesting to note that the wing-body data of references 11 to 14 at Mach numbers of 1.61 and 2.01 show that for wings of aspect ratio 3.5, taper ratio 0.2, and the same thin airfoil section a 47° swept wing-body configuration has approximately 6 percent lower drag due to lift than the corresponding unswept wing-body combination. Using data from references 15 and 16 and the references previously noted, it is possible to make the following rough estimate at a Mach number of 2.01 of the probable increments in drag due to lift between the present test model and the model of reference 8:

Increment due to -	$\Delta\frac{dC_D}{dC_L^2}$
Sweep	-0.02
Wing thickness	+0.01
Wing section	+0.02
Relative wing-tail interference	+0.03
Wing taper ratio	+0.01
	+0.05 higher for the present model

The difference remaining is approximately equal to the sum of the scatter of the data for both models.

A further comparison with the model of reference 16 which had a 45° swept wing of aspect ratio 4 and NACA 65A004 section indicates approximately the same drag due to lift at a Mach number of 2.01. There appears to be very little improvement in increasing the wing aspect ratio from 3 to 4 at a Mach number of 2.01.

Total Normal Force and Pitching Moment

Figures 6 to 8 present plots of normal-force and pitching-moment coefficients and summarize the variation of the normal-force-curve and pitching-moment-curve slopes with Mach number. Figure 6 shows that the variation of normal-force coefficient with angle of attack is linear within the range tested. The variation of pitching-moment coefficient with normal-force coefficient presented in figure 7 is also linear. The variation of the normal-force-curve slope C_{N_α} with Mach number presented in figure 8(a) is similar to the variations for the models of

references 8 and 9. At the same angle of attack, the swept-wing model develops only about 75 percent of the lift of the unswept wing model of reference 8. The variation of the static stability parameter $\frac{dC_m}{dC_N}$ with Mach number is shown in figure 8(b). In contrast to the model of reference 8, the static stability of the swept-wing model decreased gradually with increasing supersonic Mach number. At a Mach number of 2.0, the aerodynamic center of both models was approximately at the same location along the body. It is indicated that there should be some intermediate value of wing sweep that would give little or no change in static stability due to change in supersonic Mach number for an unswept, inline tail configuration.

Wing Normal-Force-Curve Slope

Figures 9, 10, and 11 pertain to the wing normal-force-curve slope. Although the test wing was of solid steel and low aspect ratio, the large amount of sweepback, thin airfoil section, and high dynamic test pressures made an estimate of the effects of wing elasticity on lift necessary. Figure 9 shows the streamwise wing twist due to a static concentrated load applied at 0.50 chord at four locations along the semispan. The method explained in reference 17 was used to calculate the ratio between the slopes of the normal-force curves for the elastic wing and the rigid wing. The results are shown in figure 10 for different values of the loading parameter $q\left(C_{N_\alpha}\right)_r$ where $\left(C_{N_\alpha}\right)_r$ is the normal-force-curve slope for the rigid wing. Figure 11 presents the wing normal-force-curve slope. The curve for the elastic wing with interference was determined from figure 8 as the difference between the swept-wing test model and the wingless model of reference 9. It should be noted that the wing lift obtained in this manner includes the interference of the body on the wing and the wing on the body and tail. Figures 10 and 3(a) were used in correcting to the rigid wing. The dashed-line curve was calculated from the wing-alone theory of references 18 and 19 and also from an unpublished extension to the wing-body interaction theory of reference 20. For the present model the wing-alone and the wing-body theories gave nearly identical results for the force-curve slope variation with Mach number, and therefore only one curve is shown. The theoretical estimates are approximately 25 percent higher than the corrected rigid-wing values. The point at a Mach number of 2.01 was obtained from the data presented in figure 10(a) of reference 16 for an aspect-ratio-4, 45° swept wing-body combination and includes a small additional lift due to the body. As would be expected at this Mach number when the wing leading edge is supersonic, the aspect-ratio-4 wing gives very nearly the same lift as the aspect-ratio-3 wing used in the present test.

Flow Conditions at the Horizontal Tail

Effective upwash at the horizontal tail surface was determined at the start of each tail flip when the lift on the tail was assumed to be zero. The following equation was used to evaluate the upwash:

$$\text{Upwash} \approx -\alpha_{\text{Flip}} - \delta$$

Figure 12 shows that for Mach numbers above 1.5 upwash occurred at the horizontal tail at angles of attack near $\pm 1^{\circ}$.

Figure 13 shows the pressure loss at the exposed mean aerodynamic chord of the horizontal tail that occurred when the tail passed through the wake from the wing. The loss decreases with increasing Mach number. Figure 14 shows that the maximum loss of effective dynamic pressure at the horizontal tail varied uniformly from 18 percent of the free-stream dynamic pressure at a Mach number of 1.4 to 10 percent at a Mach number of 2.2. The loss was slightly greater for the 3-percent-thick unswept-wing model of reference 8.

Cross Coupling

The sideslip motion that was induced by continuous pitching of the model did not build up as sharply as for the unswept-wing model of reference 8 for which maximum sideslip occurred at low supersonic Mach numbers. For the present swept-wing model a maximum amplitude in sideslip of about $\pm 2\frac{1}{2}^{\circ}$ occurred at a Mach number of 2 each time the model traversed this Mach number region. The sideslip amplitude at a Mach number of 1.4 was about 40 percent lower. The sudden variation of sideslip increment ($\Delta\beta$) shown in figure 13 of reference 8 was not so well defined for the present model. The periods of oscillation in pitch and sideslip were the same. The sideslip angle β was very nearly equal to zero at maximum angle of attack and vice versa.

CONCLUDING REMARKS

An investigation of lift, drag, and stability of a rocket-propelled model having a 52.5° swept wing of aspect ratio 3, taper ratio 0.2, and NACA 65A004 airfoil section, and inline tail surfaces leads to the following observations:

1. Drag at zero lift was nearly the same as for a model having the same body-tail and a 3-percent-thick unswept wing of hexagonal section and aspect ratio 3 (reported in NACA RM L55B10), but drag due to lift was approximately 11 to 25 percent higher.

2. The variation of lift with angle of attack was linear over the angle-of-attack test range of $\pm 5.5^{\circ}$. The variation of pitching moment with lift was also linear.

3. Static stability decreased gradually with increasing Mach number.

4. Upwash occurred at the horizontal tail at Mach numbers above 1.5 and angles of attack near $\pm 1^{\circ}$. The maximum loss of effective dynamic pressure at the horizontal tail due to the wing wake was approximately 14 percent of the free-stream dynamic pressure.

5. The continuous pitching of the model induced lateral oscillations having a maximum amplitude of about $\pm 2\frac{1}{2}^{\circ}$ of sideslip at Mach number 2.

Langley Aeronautical Laboratory,
National Advisory Committee for Aeronautics,
Langley Field, Va., August 31, 1955.

REFERENCES

1. Cohen, Clarence B.: Influence of Leading-Edge Suction on Lift-Drag Ratios of Wings at Supersonic Speeds. NACA TN 1718, 1948.

2. Polhamus, Edward C.: Drag Due to Lift at Mach Numbers up to 2.0. NACA RM L53I22b, 1953.

3. Hatch, John E., Jr., and Gallagher, James J.: Aerodynamic Characteristics of a 68.4° Delta Wing at Mach Numbers of 1.6 and 1.9 Over a Wide Reynolds Number Range. NACA RM L53I08, 1953.

4. Brown, Clinton E., and Hargrave, L. K.: Investigation of Minimum Drag and Maximum Lift-Drag Ratios of Several Wing-Body Combinations Including a Cambered Triangular Wing at Low Reynolds Numbers and at Supersonic Speeds. NACA RM L51E11, 1951.

5. Hall, Charles F.: Lift, Drag, and Pitching Moment of Low-Aspect-Ratio Wings at Subsonic and Supersonic Speeds. NACA RM A53A30, 1953.

6. Burrows, Dale L., and Palmer, William E.: A Transonic Wind-Tunnel Investigation of the Force and Moment Characteristics of a Plane and a Cambered 3-Percent-Thick Delta Wing of Aspect Ratio 3 on a Slender Body. NACA RM L54H25, 1954.

7. Burrows, Dale L., and Tucker, Warren A.: A Transonic Wind-Tunnel Investigation of the Static Longitudinal Characteristics of a 3-Percent-Thick, Aspect-Ratio-3, Delta Wing Cambered and Twisted for High Lift-Drag Ratios. NACA RM L55F02a, 1955.

8. Gillespie, Warren, Jr.: Lift, Drag, and Longitudinal Stability at Mach Numbers From 0.8 to 2.1 of a Rocket-Powered Model Having a Tapered Unswept Wing of Aspect Ratio 3 and Inline Tail Surfaces. NACA RM L55B10, 1955.

9. Gillespie, Warren, Jr., and Dietz, Albert E.: Rocket-Powered Model Investigation of Lift, Drag, and Stability of a Body-Tail Configuration at Mach Numbers From 0.8 to 2.3 and Angles of Attack Between ±6.5°. NACA RM L54C04, 1954.

10. Gillespie, Warren, Jr.: Free-Flight Determination of Force and Stability Characteristics of an Inclined Body of Fineness Ratio 16.9 at a Mach Number of 1.74. NACA RM L54G28a, 1954.

11. Robinson, Ross B.: Aerodynamic Characteristics at Supersonic Speeds of a Series of Wing-Body Combinations Having Cambered Wings With an Aspect Ratio of 3.5 and a Taper Ratio of 0.2 - Effects of Sweep Angle and Thickness Ratio on the Aerodynamic Characteristics in Pitch at M = 2.01. NACA RM L52E09, 1952.

12. Robinson, Ross B., and Driver, Cornelius: Aerodynamic Characteristics at Supersonic Speeds of a Series of Wing-Body Combinations Having Cambered Wings With an Aspect Ratio of 3.5 and a Taper Ratio of 0.2 - Effects of Sweep Angle and Thickness Ratio on the Aerodynamic Characteristics in Pitch at M = 1.60. NACA RM L51K16a, 1952.

13. Cooper, Morton, and Sevier, John R., Jr.: Effects of a Series of Inboard Plan-Form Modifications on the Longitudinal Characteristics of Two 47° Sweptback Wings of Aspect Ratio 3.5, Taper Ratio 0.2, and Different Thickness Distributions at Mach Numbers of 1.61 and 2.01. NACA RM L53E07a, 1953.

14. Sevier, John R., Jr.: Effects of a Series of Inboard Plan-Form Modifications on the Longitudinal Characteristics of Two Unswept Wings of Aspect Ratio 3.5, Taper Ratio 0.2, and Different Thickness Distributions at Mach Numbers of 1.61 and 2.0. NACA RM L53K11, 1954.

15. Knechtel, Earl D., and Summers, James L.: Effects of Sweep and Taper Ratio on the Longitudinal Characteristics of an Aspect Ratio 3 Wing-Body Combination at Mach Numbers From 0.6 to 1.4. NACA RM A55A03, 1955.

16. Spearman, M. Leroy, Driver, Cornelius, and Hughes, William C.: Investigation of Aerodynamic Characteristics in Pitch and Sideslip of a 45° Sweptback-Wing Airplane Model With Various Vertical Locations of Wing and Horizontal Tail - Basic-Data Presentation, M = 2.01. NACA RM L54L06, 1955.

17. Vitale, A. James: Effects of Wing Elasticity on the Aerodynamic Characteristics of an Airplane Configuration Having 45° Sweptback Wings As Obtained From Free-Flight Rocket-Model Tests at Transonic Speeds. NACA RM L52L30, 1953.

18. Malvestuto, Frank S., Jr., Margolis, Kenneth, and Ribner, Herbert S.: Theoretical Lift and Damping in Roll at Supersonic Speeds of Thin Sweptback Tapered Wings With Streamwise Tips, Subsonic Leading Edges, and Supersonic Trailing Edges. NACA Rep. 970, 1950. (Supersedes NACA TN 1860.)

19. Harmon, Sidney M., and Jeffreys, Isabella: Theoretical Lift and Damping in Roll of Thin Wings With Arbitrary Sweep and Taper at Supersonic Speeds - Supersonic Leading and Trailing Edges. NACA TN 2114, 1950.

20. Tucker, Warren A.: A Method for Estimating the Components of Lift of Wing-Body Combinations at Supersonic Speeds. NACA RM L52D22, 1952.

TABLE I.- CONTOUR ORDINATES OF NOSE

Station, in. from nose	Body radius, in.
0	0.17
.06	.18
.12	.21
.24	.22
.48	.28
.73	.35
1.22	.46
2.00	.64
2.45	.73
4.80	1.24
7.35	1.72
8.00	1.85
9.80	2.15
12.25	2.50
13.12	2.61
14.37	2.75
14.70	2.78
17.15	3.01
19.60	3.22
22.05	3.38
24.50	3.50
25.00	3.50

TABLE II.- CHARACTERISTICS OF MODEL

Wing:	
Span, ft	3.46
Area, sq ft	4.0
Aspect ratio	3.0
Taper ratio	0.2
Sweepback of 0.25 chord, deg	52.5
Mean aerodynamic chord, ft	1.32
Airfoil section, streamwise	NACA 65A004
Body:	
Maximum diameter, ft	0.58
Base diameter, ft	0.42
Length, ft	9.85
Fineness ratio	16.9
Boattail angle, deg	2.16
Horizontal tail:	
Span	1.85
Aspect ratio	2.7
Sweepback of 0.50 chord, deg	0
Airfoil section	4 percent hexagonal
Vertical tail:	
Span, ft	1.67
Aspect ratio	1.08
Sweepback of leading edge, deg	70
Sweepback of trailing edge, deg	15
Airfoil section	1/4-inch beveled flat plate
Model weight, lb -	
With sustainer rocket loaded	197.1
With sustainer rocket empty	153.2
Moment of inertia in pitch, slug-ft^2 -	
With sustainer rocket loaded	26.7
With sustainer rocket empty	23.8
Center of gravity with sustainer rocket loaded or empty, percent $\bar{c}$ aft of leading edge of mean aerodynamic chord	55

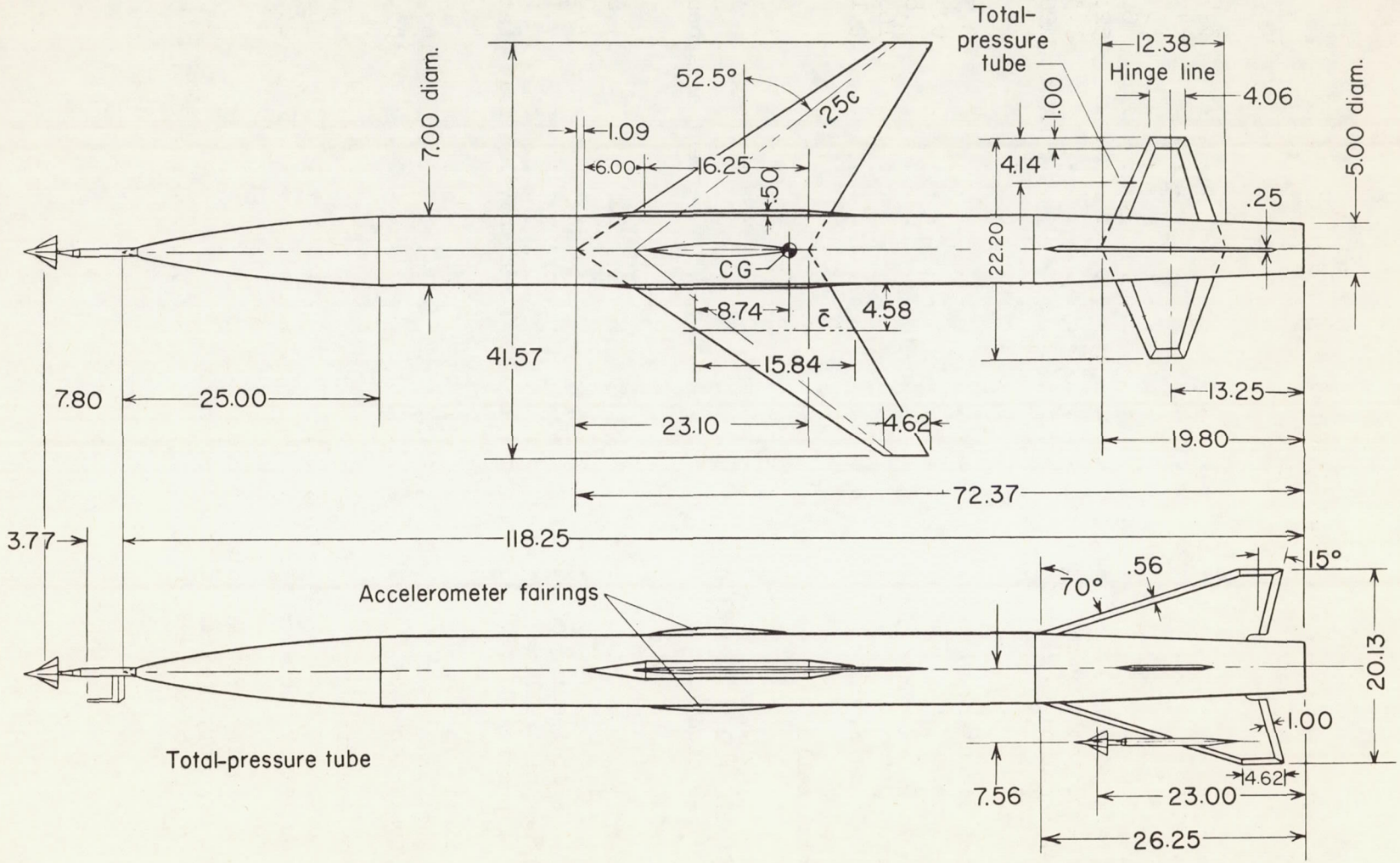

Figure 1.- Test configuration. All linear dimensions are in inches.

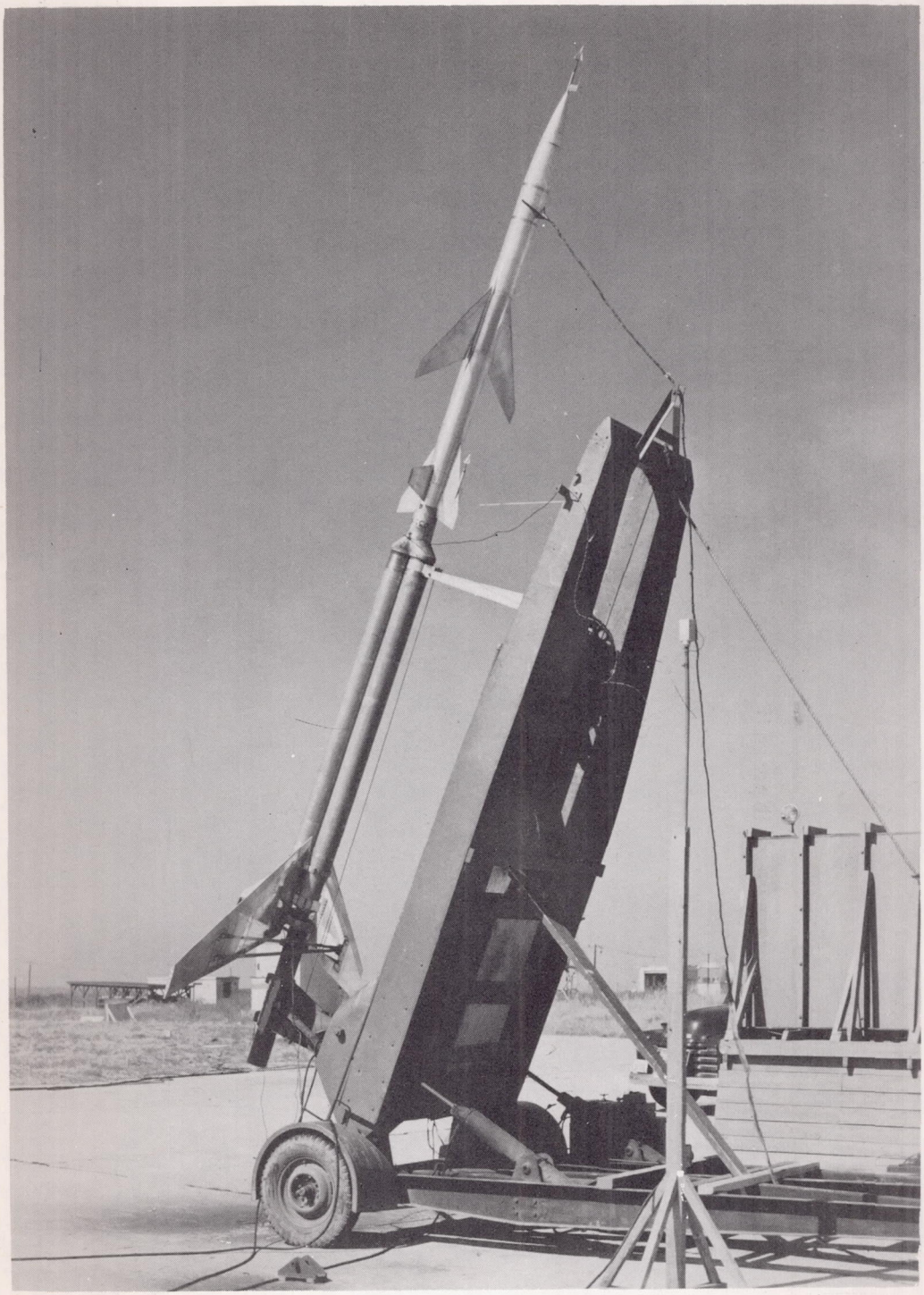

Figure 2.- Model and booster. L-84679.1

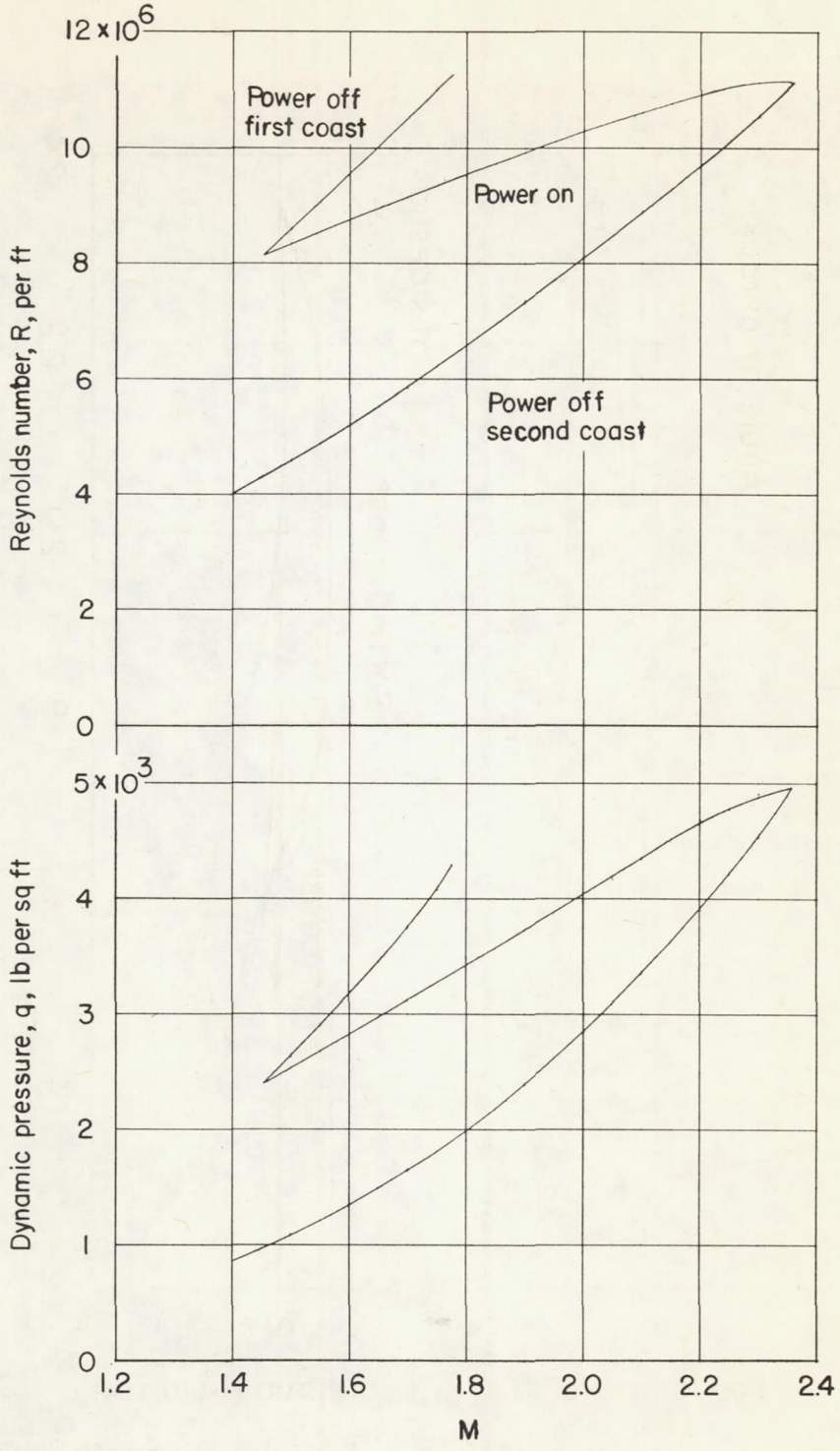

(a) Reynolds number and dynamic pressure.

Figure 3.- Flight test conditions.

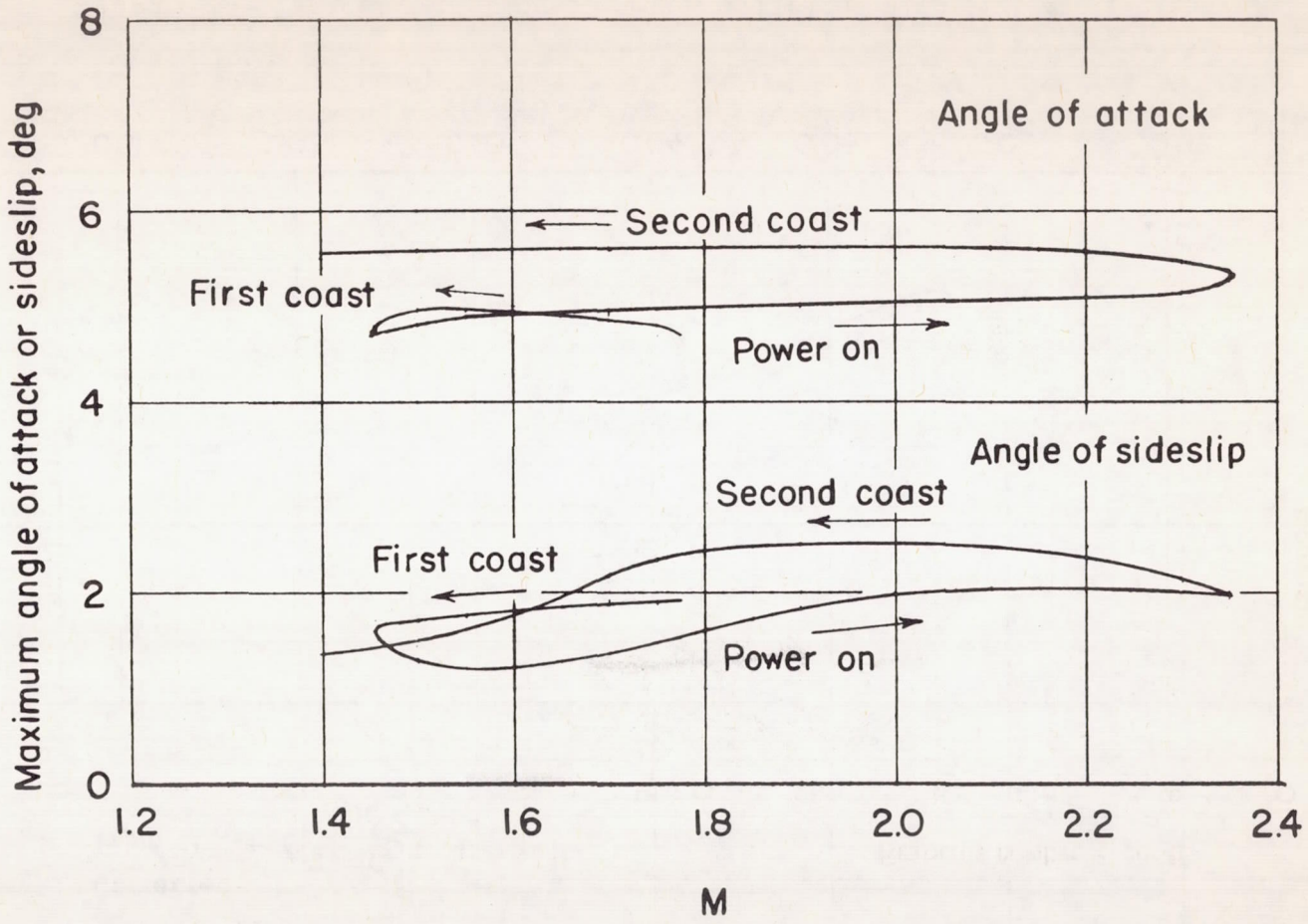

(b) Maximum angles of attack and induced sideslip.

Figure 3.- Concluded.

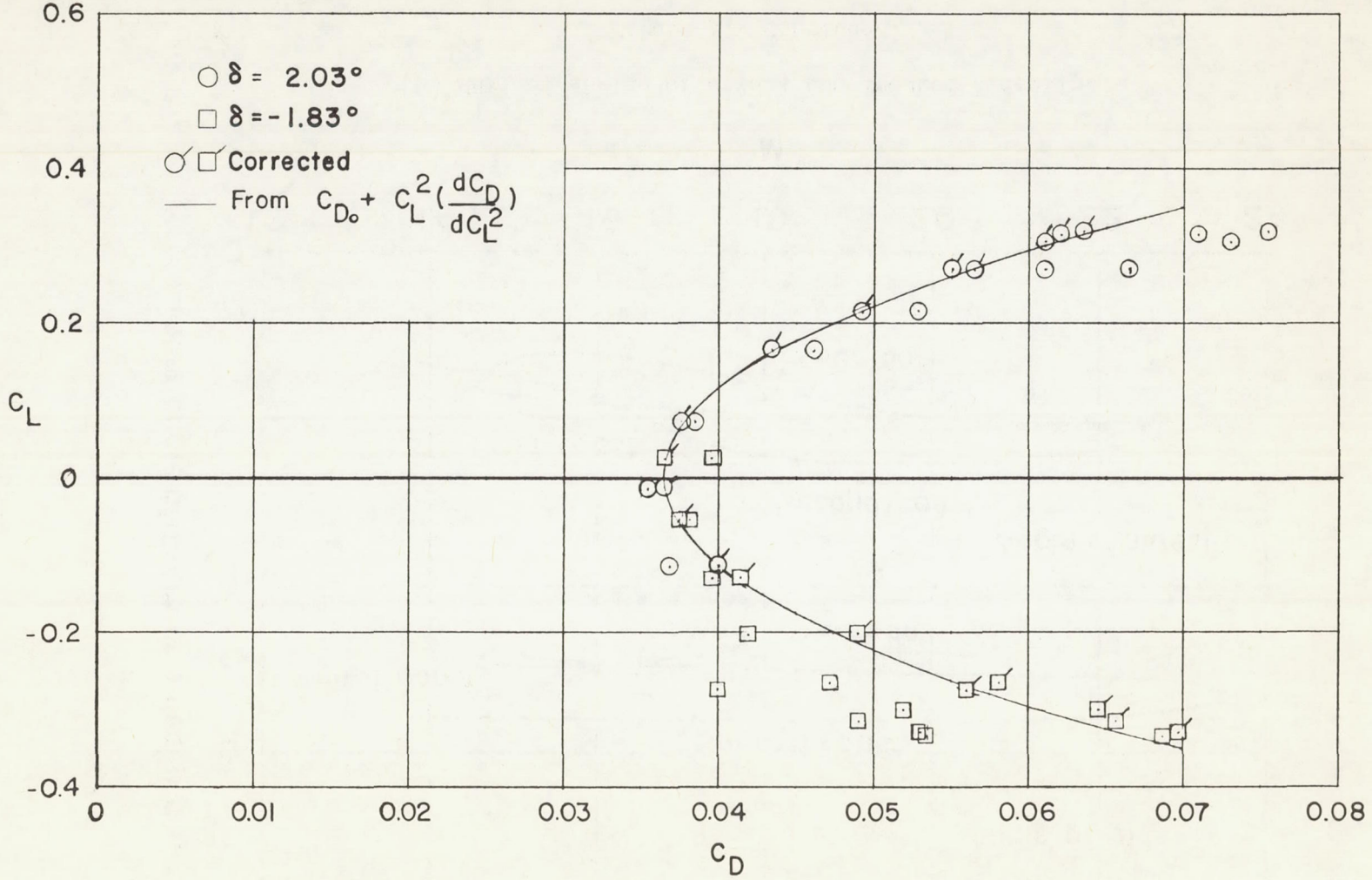

Figure 4.- Typical variation of drag coefficient with lift coefficient.

Mach number, 1.50.

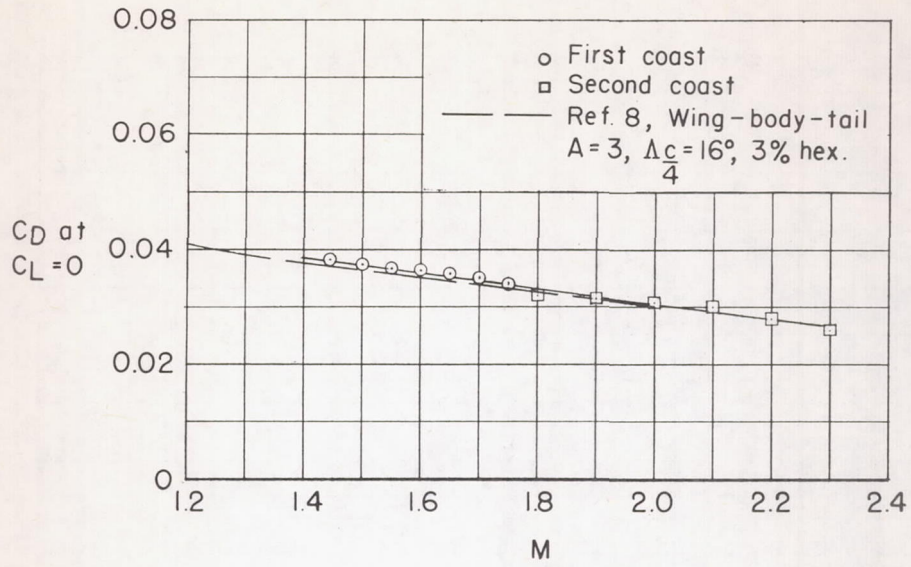

(a) Drag coefficient at $C_L = 0$.

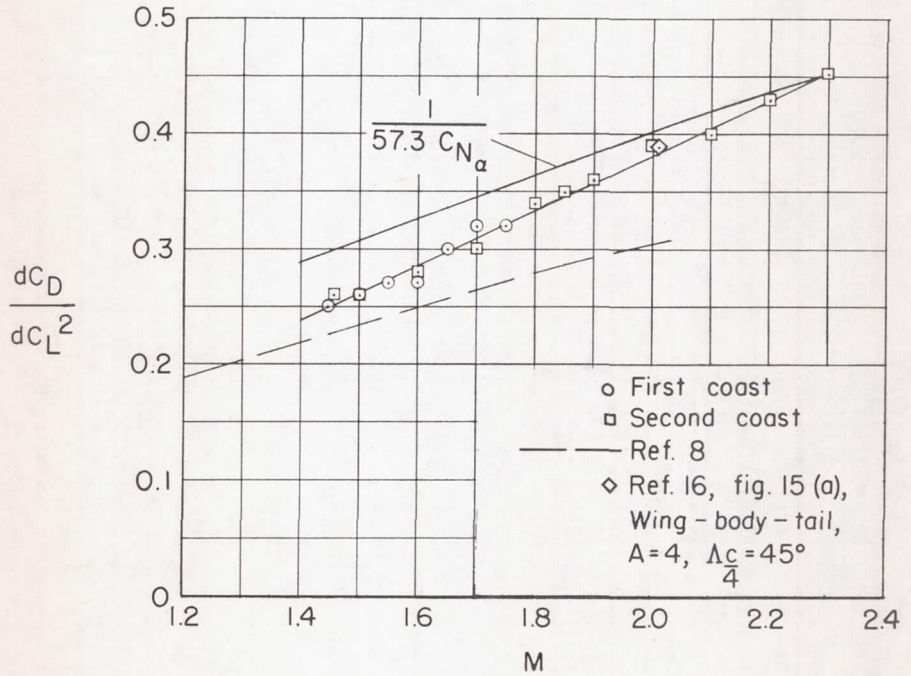

(b) Drag due to lift $\frac{dC_D}{dC_L^2}$.

Figure 5.- Variation of zero-lift drag coefficient and drag due to lift with Mach number.

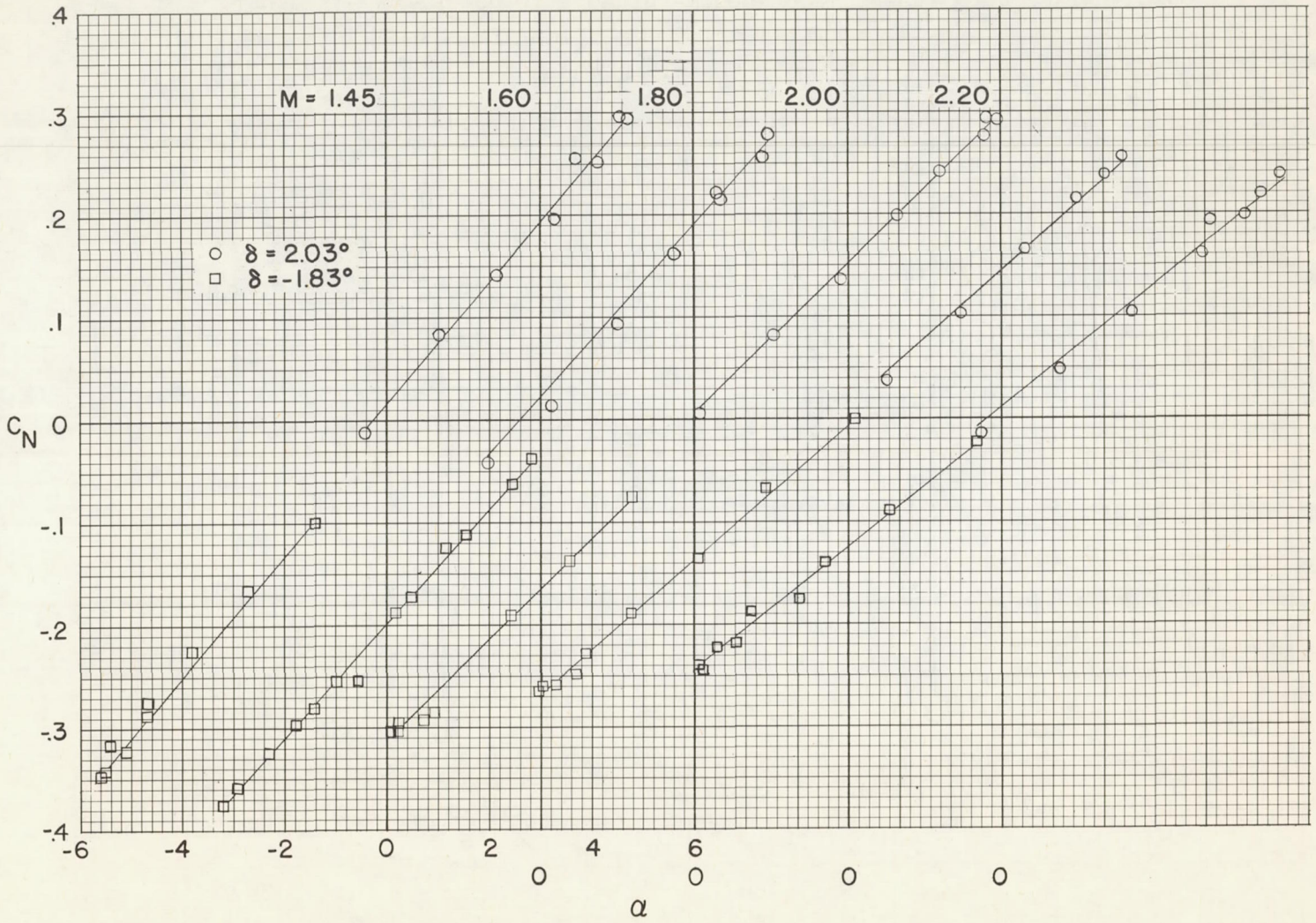

Figure 6.- Variation of normal-force coefficient with angle of attack.

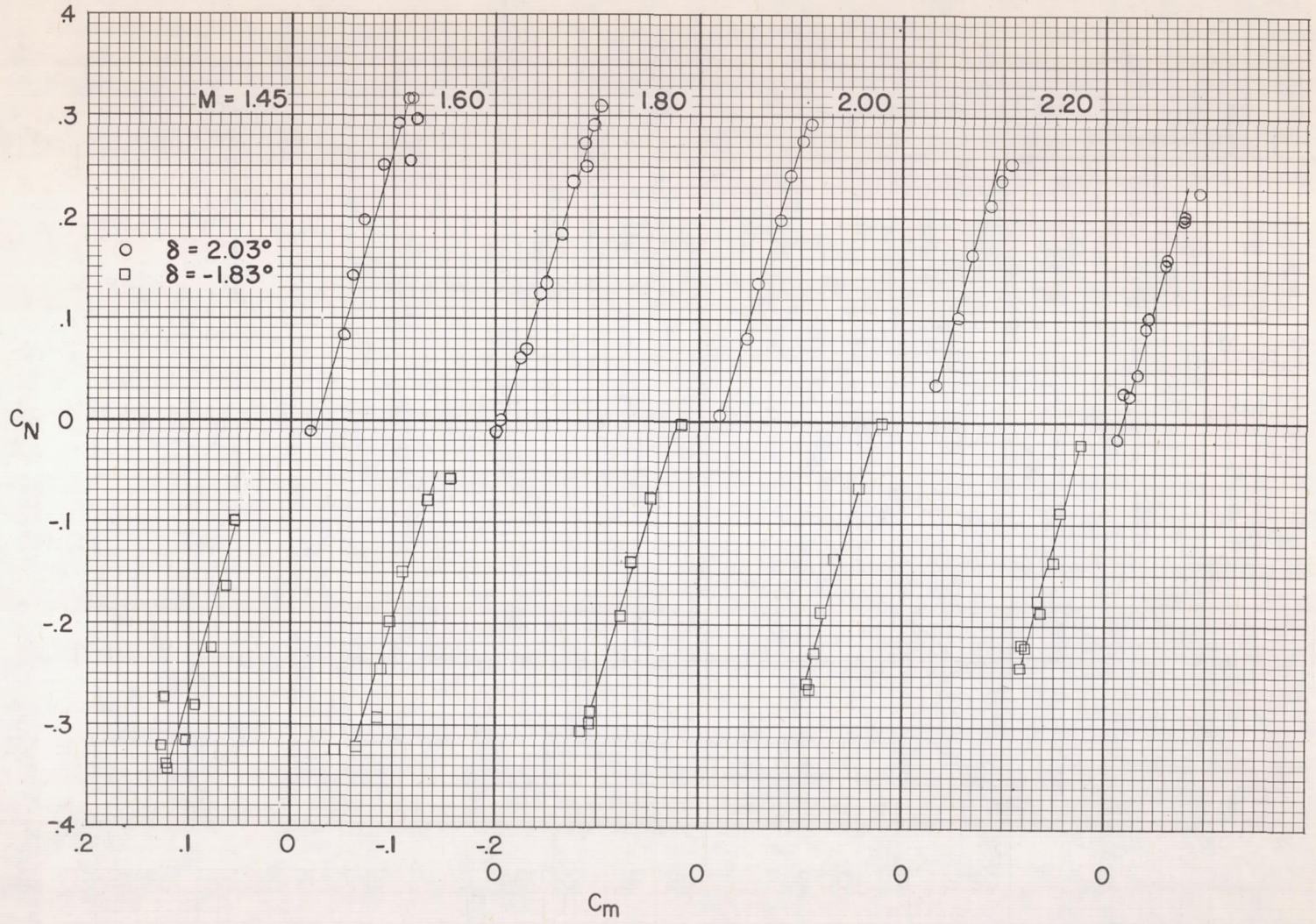

Figure 7.- Variation of pitching-moment coefficient with normal-force coefficient.

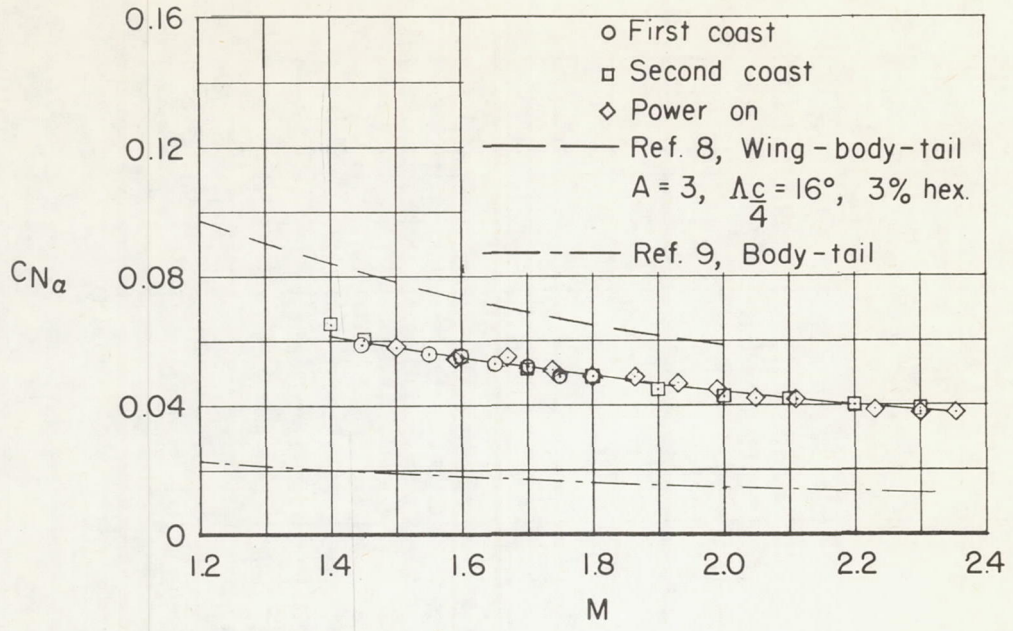

(a) Normal-force-curve slope C_{N_α}.

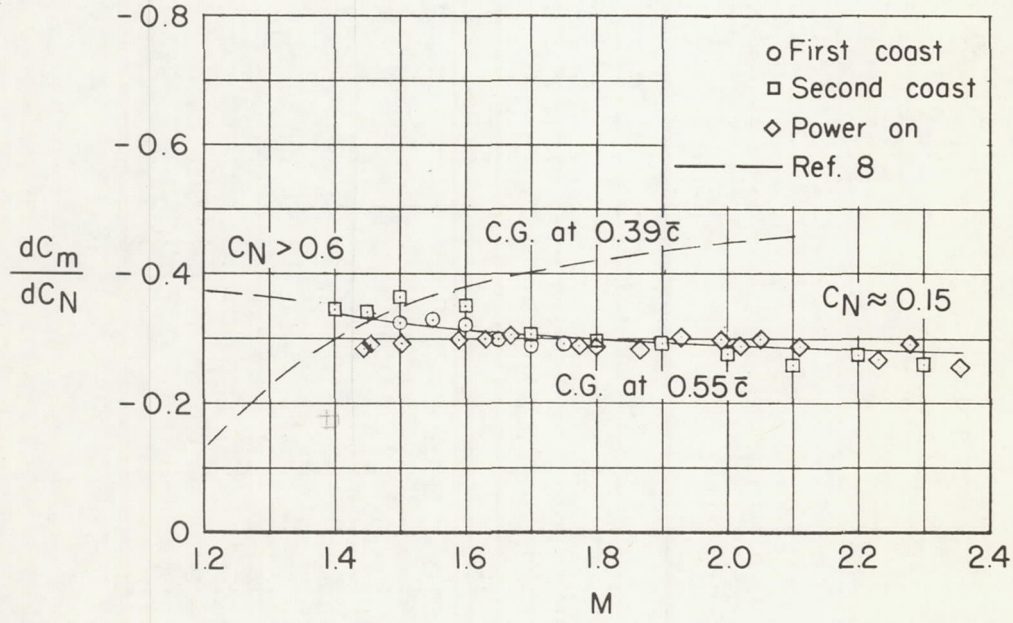

(b) Static stability parameter $\frac{dC_m}{dC_N}$.

Figure 8.- Coasting and power-on values of C_{N_α} and $\frac{dC_m}{dC_N}$.

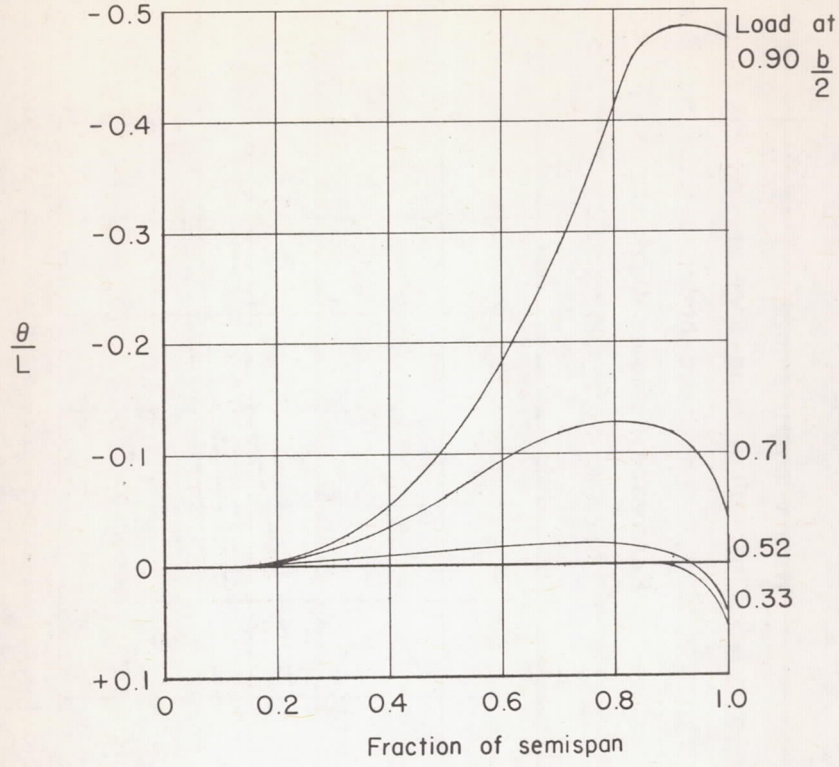

Figure 9.- Streamwise wing twist due to 100-pound load at 0.50 chord.

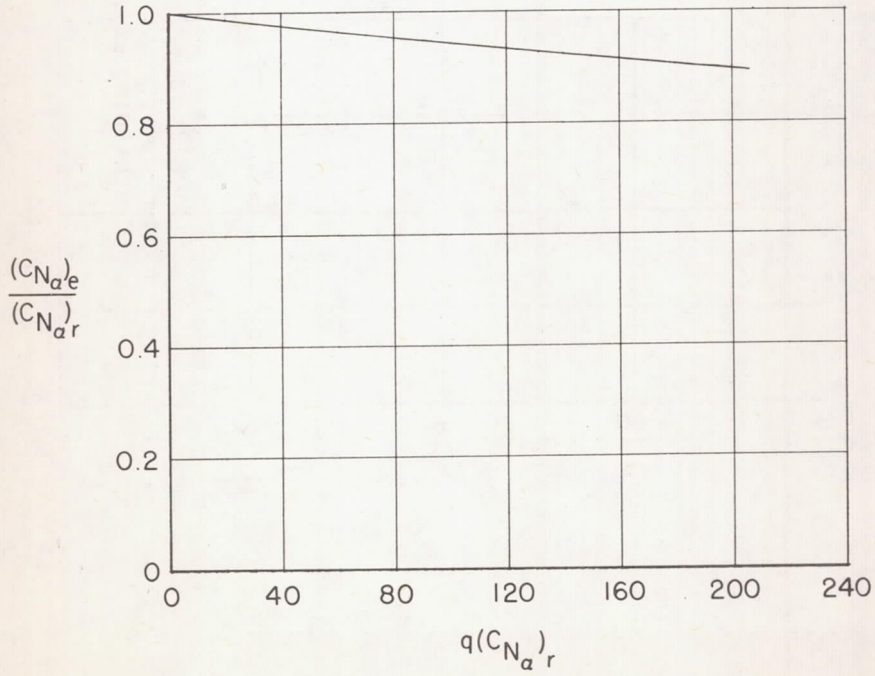

Figure 10.- Calculated elastic-to-rigid wing normal-force-curve slope ratio.

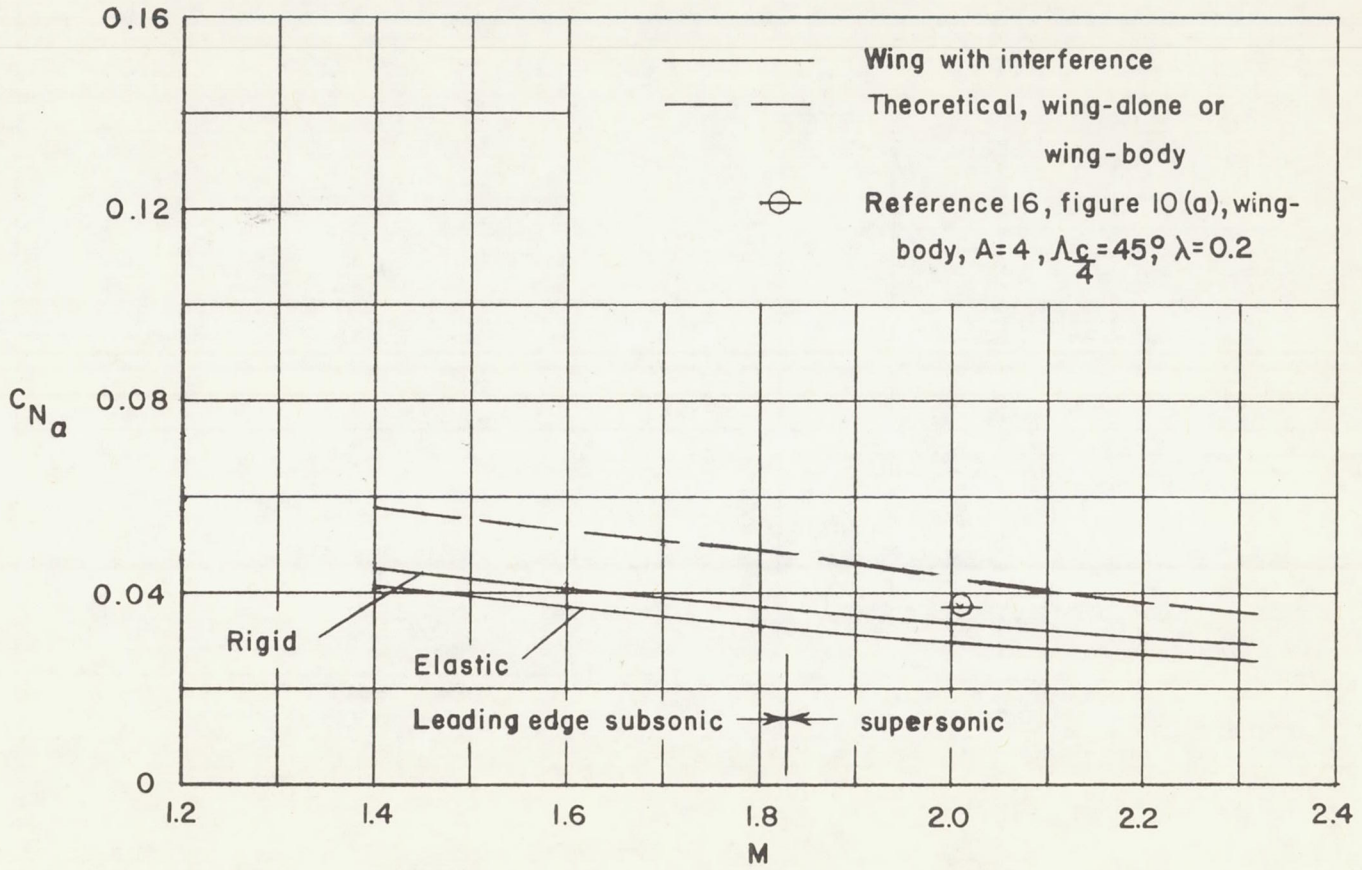

Figure 11.- Wing normal-force-curve slope.

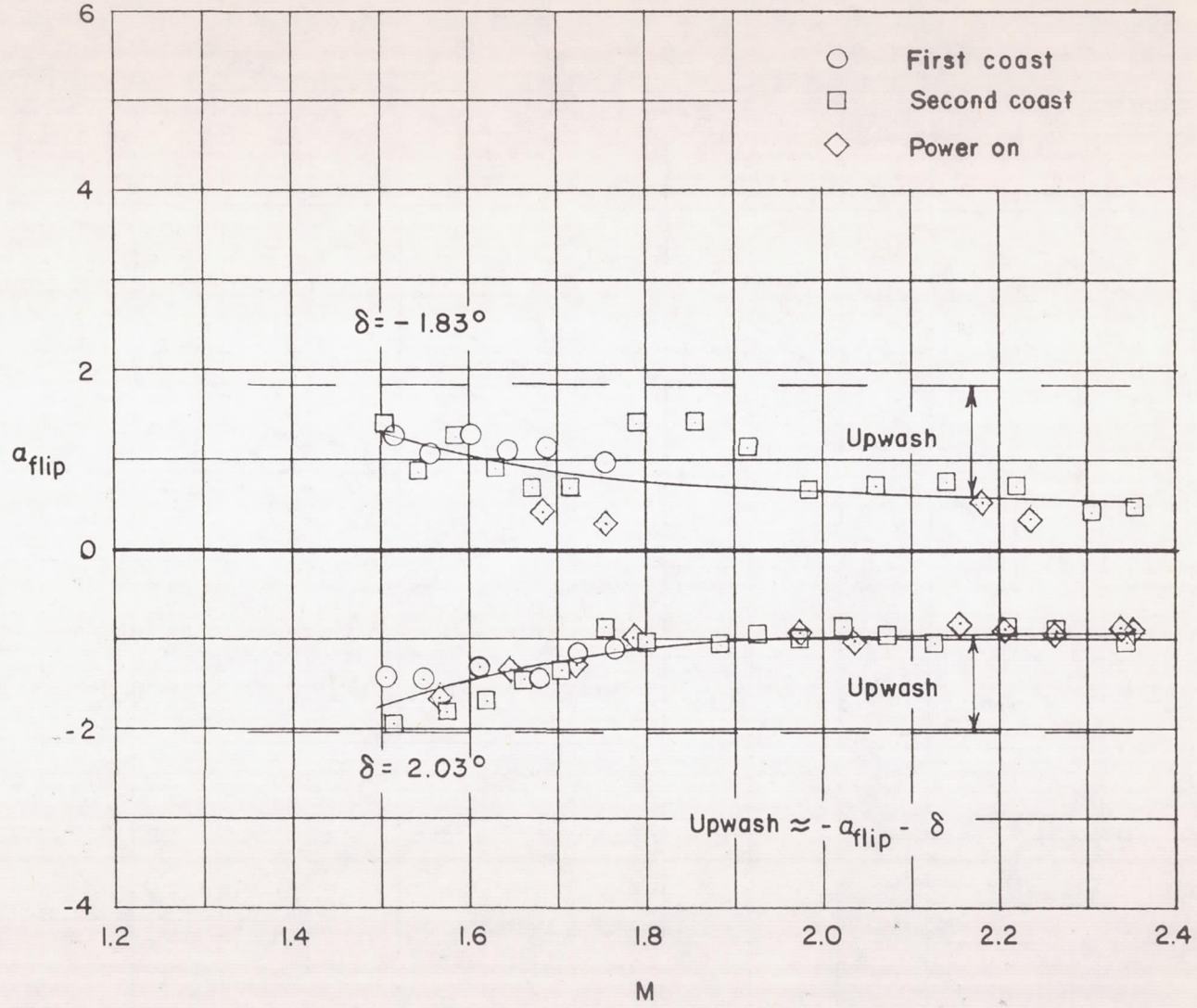

Figure 12.- Upwash indicated by start of tail flip.

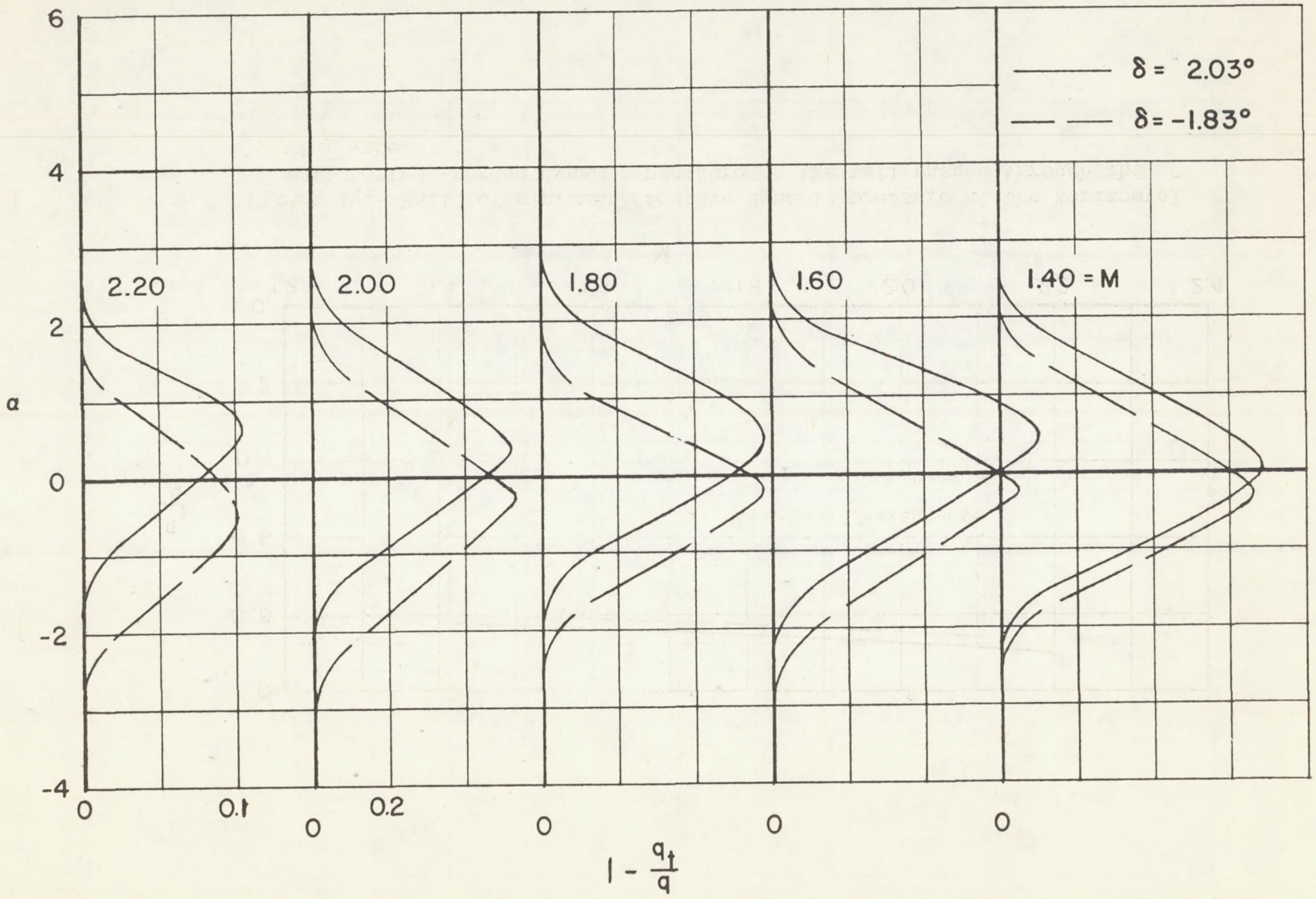

Figure 13.- Pressure loss at the horizontal tail.

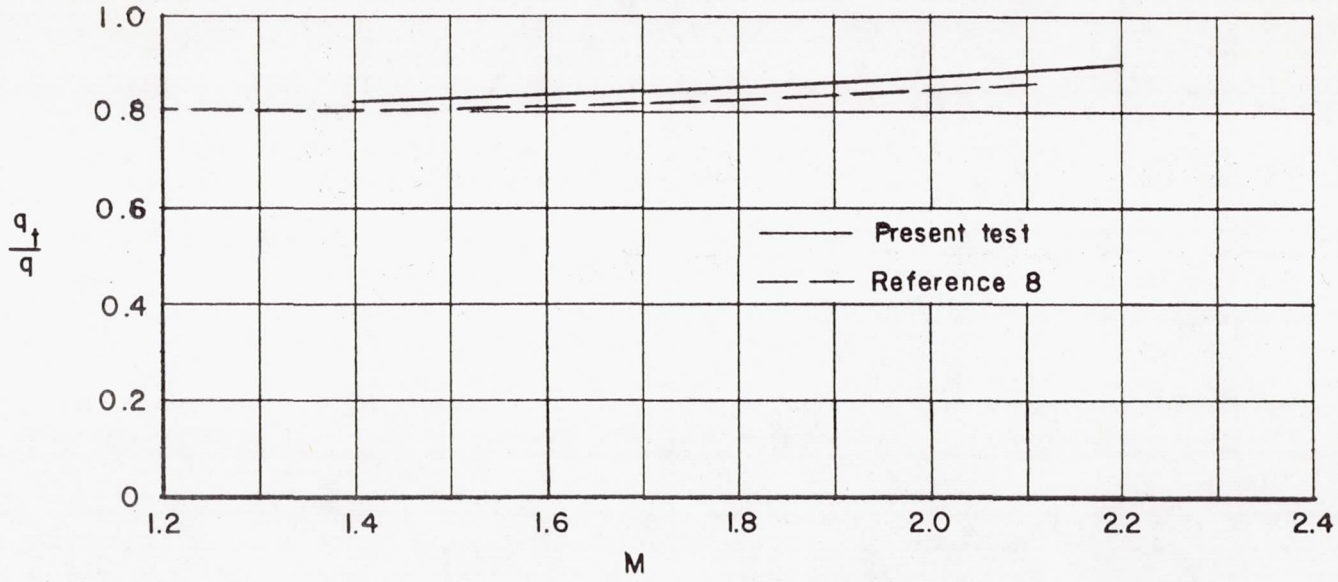

Figure 14.- Ratio of minimum effective dynamic pressure at the horizontal tail to free-stream dynamic pressure as the tail passed through the wing wake.